Protein Science (1992), *1*, 1494–1507. Cambridge University Press. Printed in the USA.

X-ray crystal structures of the oxidized and reduced forms of the rubredoxin from the marine hyperthermophilic archaebacterium *Pyrococcus furiosus*

MICHAEL W. DAY,[1] BARBARA T. HSU,[1] LEEMOR JOSHUA-TOR,[1] JAE-BUM PARK,[2] ZHI HAO ZHOU,[2] MICHAEL W.W. ADAMS,[2] AND DOUGLAS C. REES[1]

[1] Division of Chemistry and Chemical Engineering, California Institute of Technology, Pasadena, California 91125
[2] Department of Biochemistry and Center for Metalloenzyme Studies, University of Georgia, Athens, Georgia 30602

(RECEIVED April 29, 1992; REVISED MANUSCRIPT RECEIVED June 9, 1992)

Abstract

The structures of the oxidized and reduced forms of the rubredoxin from the archaebacterium, *Pyrococcus furiosus*, an organism that grows optimally at 100 °C, have been determined by X-ray crystallography to a resolution of 1.8 Å. Crystals of this rubredoxin grow in space group $P2_12_12_1$ with room temperature cell dimensions a = 34.6 Å, b = 35.5 Å, and c = 44.4 Å. Initial phases were determined by the method of molecular replacement using the oxidized form of the rubredoxin from the mesophilic eubacterium, *Clostridium pasteurianum*, as a starting model. The oxidized and reduced models of *P. furiosus* rubredoxin each contain 414 nonhydrogen protein atoms comprising 53 residues. The model of the oxidized form contains 61 solvent H_2O oxygen atoms and has been refined with X-PLOR and TNT to a final R = 0.178 with root mean square (rms) deviations from ideality in bond distances and bond angles of 0.014 Å and 2.06°, respectively. The model of the reduced form contains 37 solvent H_2O oxygen atoms and has been refined to R = 0.193 with rms deviations from ideality in bond lengths of 0.012 Å and in bond angles of 1.95°. The overall structure of *P. furiosus* rubredoxin is similar to the structures of mesophilic rubredoxins, with the exception of a more extensive hydrogen-bonding network in the β-sheet region and multiple electrostatic interactions (salt bridge, hydrogen bonds) of the Glu 14 side chain with groups on three other residues (the amino-terminal nitrogen of Ala 1; the indole nitrogen of Trp 3; and the amide nitrogen group of Phe 29). The influence of these and other features upon the thermostability of the *P. furiosus* protein is discussed.

Keywords: electron transfer proteins; protein stability; protein structure; rubredoxin; thermostability

Rubredoxins are non-heme iron proteins of low molecular weight that occur in several anaerobic bacteria. Rubredoxin is thought to participate in electron transfer reactions, but little is known about its specific physiological functions. In contrast to the paucity of information regarding the biological function of rubredoxin, much more is known about its three-dimensional structure. The high resolution X-ray structures of four rubredoxins from mesophilic bacteria have been reported with Brookhaven Protein Data Bank (Bernstein et al., 1977; Abola et al., 1987) identifiers given in brackets: *Clostridium pasteurianum* (RdCp [5RXN], 1.2 Å resolution) (Watenpaugh et al., 1979), *Desulfovibrio gigas* (RdDg [1RDG], 1.4 Å resolution) (Frey et al., 1987), *Desulfovibrio desulfuricans* (RdDd [6RXN], 1.5 Å resolution) (Sieker et al., 1986), and *Desulfovibrio vulgaris* (RdDv [7RXN], 1.5 Å resolution) (Adman et al., 1991). These rubredoxins are structurally similar to each other, with a tetrahedral array of four cysteine sulfur atoms ligating a single iron atom. They typically consist of 52–54 amino acid residues folded into a short three-stranded antiparallel β-sheet and a number of loops. The sequences of 13 rubredoxins are known (see Fig. 1).

Pyrococcus furiosus is an anaerobic sulfur-reducing archaebacterium that is found near submarine geothermal vents on the ocean floor (Fiala & Stetter, 1986). With an

Reprint requests to: Douglas C. Rees, Division of Chemistry and Chemical Engineering 147-75CH, California Institute of Technology, Pasadena, California 91125.

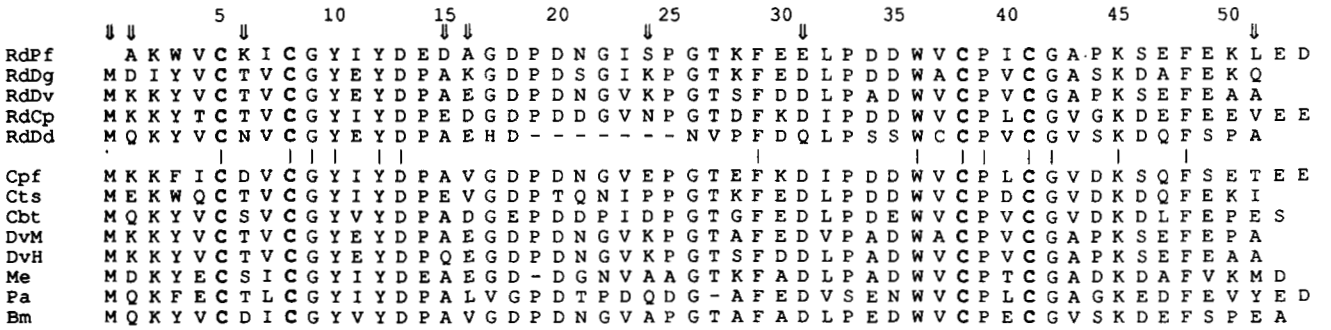

Fig. 1. Sequence alignment for the rubredoxins from anaerobic bacteria (Blake et al., 1991). The top five sequences are for the rubredoxins whose X-ray structures have been solved. The conserved cysteines are given in boldface. The symbols ⇓ and | indicate residues that are unique to RdPf and residues that are strictly conserved in all known rubredoxins, respectively. Residue numbers correspond to the RdPf sequence, which has one less residue at the amino-terminus than the other rubredoxins. The abbreviations and references are: RdPf, *Pyrococcus furiosus* (Blake et al., 1991); RdDg, *Desulfovibrio gigas* (Bruschi, 1976a); RdDv, *Desulfovibrio vulgaris* (Bruschi, 1976b); RdCp, *Clostridium pasteurianum* (Watenpaugh et al., 1973; Yasunobo & Tanaka, 1983); RdDd, *Desulfovibrio desulfuricans* (Hormel et al., 1986); Cpf, *Clostridium perfringens* (Seki et al., 1989); Cts, *Clostridium thermosaccharolyticum* (Meyer et al., 1990); Cbt, *Chlorobium thiosulfatophilum* (Woolley et al., 1987); DvM, *D. vulgaris* strain Miyazaki (Shimizu et al., 1989); DvH, *D. vulgaris* strain Hildenborough (Bruschi, 1976b; Voordouw, 1988); Me, *Megasphaera elsdenii* (Bachmeyer et al., 1968b); Pa, *Peptococcus aerogenes* (Bachmeyer et al., 1968a); Bm, *Butyribacterium methylotrophicum* (Saeki et al., 1989).

optimal growth temperature of 100 °C, it is considered to be a hyperthermophile. As expected from the growth conditions for *P. furiosus*, the rubredoxin from this organism (RdPf) exhibits significant thermostability, as the UV-visible and EPR properties of the protein are unaffected after a 24-h incubation at 95 °C (Blake et al., 1991). In contrast, rubredoxins from mesophilic bacteria are less thermostable; RdCp is rapidly denatured at 80 °C (Lovenberg & Sobel, 1965), whereas RdDg loses 50% of its visible absorption after ~2 h at 80 °C (Papavassilou & Hatchikian, 1985). Consequently, RdPf provides the opportunity to study factors that influence the extreme thermostability of this protein and hence to examine structural features that may be important to the thermostability of proteins in general. This paper describes the three-dimensional X-ray structures of the oxidized and the reduced forms of the rubredoxin from *P. furiosus* determined at 1.8 Å. Features of the structure that may be significant to the increased stability of this protein at extreme temperatures are discussed.

Experimental

Crystallization

The growth of *P. furiosus* and the isolation of rubredoxin (RdPf) were as previously described (Bryant & Adams, 1989; Blake et al., 1991). Crystals of the oxidized form of rubredoxin were grown using the hanging drop method by equilibrating a 4-μL drop against a solution containing 30% 2-methyl-2,4-pentanediol, 2.2 M $(NH_4)_2SO_4$, and 0.1 M Tris-HCl, pH 8.5. The drop contained 2 μL of protein solution (~60 mg/mL protein, 0.3 M NaCl, and 50 mM Tris-HCl, pH 8.0) and 2 μL of buffered ammonium sulfate solution (3.2 M $(NH_4)_2SO_4$ and 0.15 M Tris-HCl, pH 8.5). Deep red rectangular crystals of approximate dimensions 0.3 × 0.3 × 0.4 mm grew overnight in the orthorhombic space group $P2_12_12_1$ with unit cell dimensions of $a = 34.6$ Å, $b = 35.5$ Å, $c = 44.4$ Å, and $V = 54{,}536$ Å^3. Assuming four molecules in the unit cell, the ratio of volume to molecular weight (Matthews, 1968), V_m, is calculated to be 2.30 Å^3/Da. At low temperature (−161 °C) the unit cell dimensions each shrink by approximately 2.5% to $a = 33.8$ Å, $b = 34.6$ Å, and $c = 43.4$ Å with a corresponding 7% loss in volume to $V = 50{,}755$ Å^3.

Crystals of the reduced form of rubredoxin were obtained by adding a minimum amount (several grains) of sodium dithionite ($Na_2S_2O_4$) to drops containing crystals of the oxidized form of rubredoxin. Upon addition of sodium dithionite, the crystals gradually lose their deep red color over a period of 1–2 min, becoming colorless and extremely fragile. When the crystals became colorless, they were removed from the drop and mounted on a glass spatula for data collection and immediately placed into a −161 °C stream of N_2. The space group and measured unit cell dimensions are virtually identical to those of the oxidized form ($P2_12_12_1$, $a = 33.8$ Å, $b = 34.5$ Å, $c = 43.2$ Å, and $V = 50{,}375$ Å^3).

Data collection

All intensity data were collected on a Siemens X-1000 area detector with the crystal to detector distance set at 8.0 cm. Cu Kα (λ = 1.5418 Å) radiation was generated by a Siemens rotating anode generator operating at 4.5 kW

(50 kV × 90 mA) with a graphite monochromator. For low temperature data collection, the crystals were cooled to −161 °C with a stream of cold nitrogen generated by a Siemens LT-2A low temperature device, employing the cryocrystallographic techniques of Hope (1988, 1990).

Data for initial phasing and model building were collected at room temperature to a maximum resolution of 2.2 Å with the detector center set at $2\theta = 10°$. Unfortunately, the crystal dissolved during data collection and it was not possible to obtain data from a second orientation. The data were integrated using XENGEN (Howard et al., 1987) and scaled using the program package ROCKS (Bethge, 1984; Reeke, 1984). The resulting data set (2,322 reflections) was 66.9% complete to 2.2 Å with R_{merge} = 8.8% (see Table 1). Data used for the refinement of the structure were collected at −161 °C from a single crystal of the oxidized form to a maximum resolution of 1.1 Å, employing two orientations of the area detector. Data to 1.8 Å resolution were collected with the detector centered at $2\theta = 20°$. Data between 2.8 Å and 1.1 Å resolution were collected with the detector at $2\theta = 60°$. The data were integrated, scaled, and merged using XENGEN, resulting in a data set (17,366 reflections) 81.2% complete to 1.1 Å with R_{merge} = 4.4% (see Table 1).

Data were collected at −161 °C from a single crystal of the reduced form to a maximum resolution of 1.5 Å with a single setting of the detector at $2\theta = 30°$. Data were integrated, scaled, and merged as above. The final data set containing 7,859 reflections is 98.7% complete to 1.6 Å and 90.9% complete to 1.5 Å with R_{merge} = 3.7%.

Structure determination

The structure of oxidized RdPf was solved by molecular replacement, using as the search model 337 atoms (excluding Fe) common to RdPf and RdCp. Rotation functions were calculated with the fast rotation function of Crowther (1972), using all measured reflections between 8 and 3 Å and integration radii varying between 12 and 20 Å. The oriented molecule was positioned in the cell by a brute-force translation search using reflections between 6.5 and 3.5 Å resolution. A solution was found with a correlation coefficient of 0.54 that was 50% greater than the next highest peak. The R-factor ($R = \Sigma ||F_o| - |F_c|| / \Sigma |F_o|$) for the rotated and translated model (calculated with the refinement package TNT [Tronrud et al., 1987]) was $R = 0.45$.

Refinement

Oxidized form

The 337 atoms of the starting model (excluding the Fe atom) were refined as a rigid body against data in the resolution range between 11 and 2.5 Å, using the refinement package TNT. The initial model rotated by less than 0.1° and translated by less than 0.002 Å along any axis, lowering the R-factor from 0.45 to 0.41. Calculation of $F_o - F_c$ and $2F_o - F_c$ maps revealed the positions of the Fe atom and 9 of the 23 residue side chains not in common with the RdCp structure. The position indicated for the Fe atom was consistent with the strongest peaks observed in the native anomalous difference Patterson map (not shown). Refinement of the new model using the geometric restraints in TNT and a single overall temperature factor yielded $R = 0.33$. Electron-density difference maps ($F_o - F_c$ and $2F_o - F_c$) revealed the positions of six more residue side chains. At this point, manual adjustments were made to the existing structure using the computer graphics program TOM (Jones, 1978). The new model was refined with TNT incorporating the 2,243 reflections between 20 and 2.2 Å resolution with a resulting R = 0.27. A subsequent set of electron-density difference maps ($F_o - F_c$ and $2F_o - F_c$) established the positions of the remaining side chains. As before, manual adjustments were made to the model as needed. Alternating refinement of positions and temperature factors for the complete model including data between 20 and 2.2 Å resulted in an R-factor of 0.25.

Table 1. *Data collection statistics*

Data set	Resolution range (Å)	Unique reflections	% Observed	Number of observations	R_{merge}
R.T.[a]	∞–2.2	2,322	66.9	7,767	0.088
−161 °C (ox)[b]	∞–1.1	17,366	81.2	78,073	0.044
$2\theta = 20°$[c]	∞–1.8	4,439	87.3	18,963	0.025
−161 °C (red)[d]	∞–1.5	7,859	90.9[e]	45,990	0.037

[a] Room temperature, oxidized RdPf data set used for the initial molecular replacement calculations.
[b] Complete oxidized RdPf data set collected at −161 °C, merging data collected with the detector center at both $2\theta = 20°$ and $2\theta = 60°$.
[c] Low temperature, oxidized RdPf data collected with the detector center set at $2\theta = 20°$ and used for structure refinement.
[d] Low temperature, reduced RdPf data collected with the detector center set at $2\theta = 30°$ and used for structure refinement.
[e] One hundred percent complete to 1.8 Å resolution.

Following the stereochemically restrained least-squares refinement of RdPf with TNT, the slow-cooling simulated-annealing protocol of X-PLOR (Brünger et al., 1987, 1990) was used for further refinement of atomic positions. Unit weights were applied to the structure factors during refinement. From a starting temperature of 4,000 K, the final temperature of 300 K was reached by decreasing the temperature in steps of 25 K every 50 fs, resulting in a residual of 0.26. Refinement of temperature factors in X-PLOR, followed by another round of simulated annealing and temperature factor refinement, lowered the R-factor to 0.20 with root mean square (rms) deviations from ideality in bond distances of 0.018 Å and in bond angles of 3.25°.

The model was further refined against the data collected at −161 °C, to a maximum resolution of 1.8 Å (4,439 reflections, 87% complete). The present refinement included all reflections with intensities greater than zero, collected with the detector centered at $2\theta = 20°$ (corresponding to a limiting resolution of 1.8 Å). Electron-density maps calculated to higher resolutions (between 1.8 Å and 1.1 Å resolution, including data collected with the detector set at $2\theta = 60°$) displayed anisotropic electron density that will require additional refinement strategies to model adequately. No significant anisotropy was observed in electron-density maps calculated at 1.8 Å resolution. At present, the structure refinement, which includes the incorporation of 61 solvent H_2O molecules (of approximately 120 possible, based on volume considerations), has resulted in a residual of $R = 0.178$, with rms deviations from ideal bond lengths of 0.014 Å and bond angles of 2.06°. The average temperature factors for the main chain and the side chain atoms are 6.6 Å^2 and 8.9 Å^2, respectively. Residues Glu 52 and Asp 53 at the C-terminus and the side chains of Lys 6, Lys 28, Glu 30, Glu 31, and Glu 49 have large average Bs (>17 Å^2) (see Fig. 2). Two conformations of the Glu 52 and Asp 53 side chains were identified, although only the major conformation for each residue was refined. The final $2F_o - F_c$ electron-density map in the region around Glu 14 is illustrated in Figure 3. Estimation of the average coordinate error from a Luzzati (1952) plot was complicated by the nearly constant value of the R-factor as a function of resolution (Fig. 4). This is possibly a consequence of applying unit weights to the structure factors during refinement (Adman, 1990). If the dependence of R on resolution is examined to a limiting resolution of 1.1 Å, where data between 1.8 Å and 1.1 Å resolution were not included in the refinement, then a Luzzati-type analysis (Srinivasan & Parthasarathy, 1976) is consistent with an average coordinate error of ~0.15 Å and a model that is ~97% complete. The missing scattering matter presumably consists of partially occupied solvent molecules that have not yet been included in the refinement.

A Ramachandran plot of the (ϕ, ψ) main chain torsion angles is shown in Figure 5. All residues have ϕ, ψ angles in allowed regions. The five residues with ϕ angles near 90° are glycines.

Reduced form

The R-factor between the data from the reduced form and the oxidized RdPf observed data to 1.8 Å is 0.43. The corresponding R-factor with the RdPf oxidized model is 0.45. Difference Fourier maps between the observed data from the reduced crystal and either the oxidized F_o's or the oxidized model F_c's were very noisy and revealed no structural differences. The model from the oxidized form, including solvent H_2O oxygen atoms, was then refined against the data from the reduced form as a rigid body resulting in $R = 0.31$. The model rotated by 2.98° and translated by up to 0.31 Å along the crystallographic axes. The stereochemically restrained individual atomic positions were refined in the next cycles, followed by refinement of the temperature factors. The resulting model with $R = 0.24$, was used to calculate $F_o - F_c$ and $2F_o - F_c$ maps to evaluate the model. Again, no gross structural

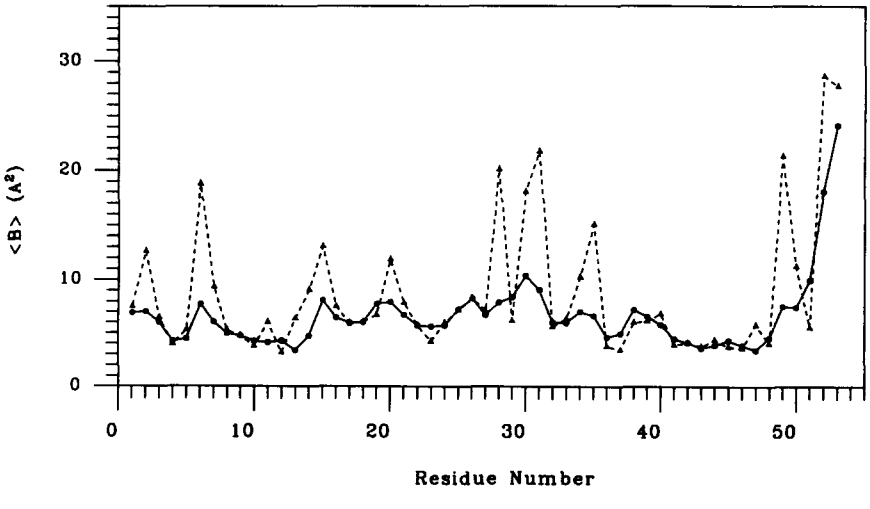

Fig. 2. Average main chain and side chain temperature factors for the oxidized form. The main chain is shown by the solid line and the side chain is shown by the dashed line.

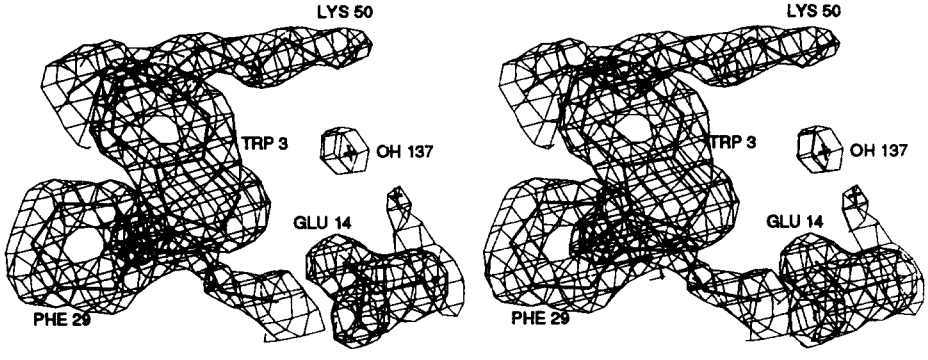

Fig. 3. Stereo view of the final $2F_o - F_c$ electron-density map in the region around Glu 14.

changes were observed, although it became apparent that the solvent region would require redetermination. A total of 24 solvent H_2O, all having either large temperature factors or questionable locations, were removed. The protein without the solvent shell was refined by simulated annealing with X-PLOR, followed by positional refinement of both the solvent shell and protein. The refinement of the reduced model was restricted to 1.8 Å resolution for consistency with the oxidized RdPf refinement. At present, the R-factor is 0.193, with rms deviations from ideal bond distances and bond angles of 0.012 Å and 1.95°, respectively. The reduced form of RdPf has average temperature factors for the main chain atoms of $B = 7.6$ Å^2 and $B = 9.9$ Å^2 for side chain atoms. The side chains of the reduced RdPf with large average temperature factors ($B > 15$ Å^2) include those mentioned above for the oxidized form and Asp 20, Glu 31, Asp 34, and Asp 35 ($B > 20$ Å^2) (see Fig. 6). In contrast to the oxidized model, the side chains of residues 52 and 53 appear to have one major conformation.

Coordinates for oxidized and reduced RdPf have been deposited with the Protein Data Bank, file numbers 1CAA and 1CAD, respectively.

Structure

Overall folding

The overall folding (see Fig. 7 and Kinemage 1) of RdPf is very similar to the other rubredoxins that have been refined to high resolution (Watenpaugh et al., 1979; Sieker et al., 1986; Frey et al., 1987; Adman et al., 1991). The structure is made up of a three-stranded antiparallel β-sheet composed of residues Ala 1 to Lys 6, Gly 9 to Glu 14, and Glu 47 to Leu 51, involving nine hydrogen bonds (see Table 2, Fig. 8, and Kinemage 4). The hydrogen-bonding pattern between the first and second β-strands is interrupted by a G1 type β bulge (Richardson et al., 1978) that occurs between residues Gly 9 and Tyr 10. The overall hydrogen-bonding pattern (see Table 2) is in close agreement with the pattern reported in the ^{1}H-NMR secondary structure analysis (Blake et al., 1991). The hydrophobic core contains six aromatic residues – Trp 3, Tyr 10, Tyr 12, Phe 29, Trp 36, and Phe 48 – as well as the hydrophobic aliphatic residue Leu 32 (see Fig. 9 and Kinemage 3). The aromatic residues in the hydrophobic core are nearly invariant among the known rubredoxin sequences (see Ta-

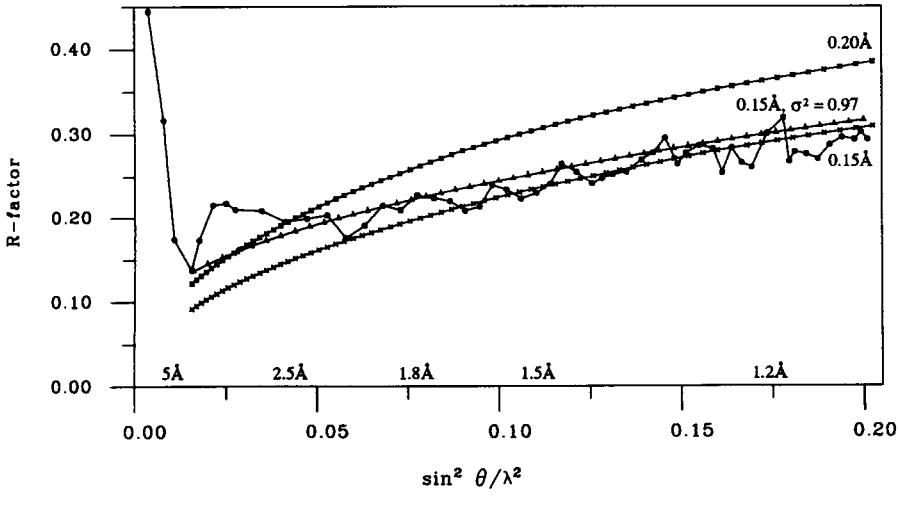

Fig. 4. Dependence of R-factor on resolution. Theoretical curves are calculated for coordinate error of 0.15 Å and 0.20 Å and for a partial model containing 97% of the scattering mass with an average coordinate error of 0.15 Å. Only reflections in the resolution range 5–1.8 Å were used in the refinement.

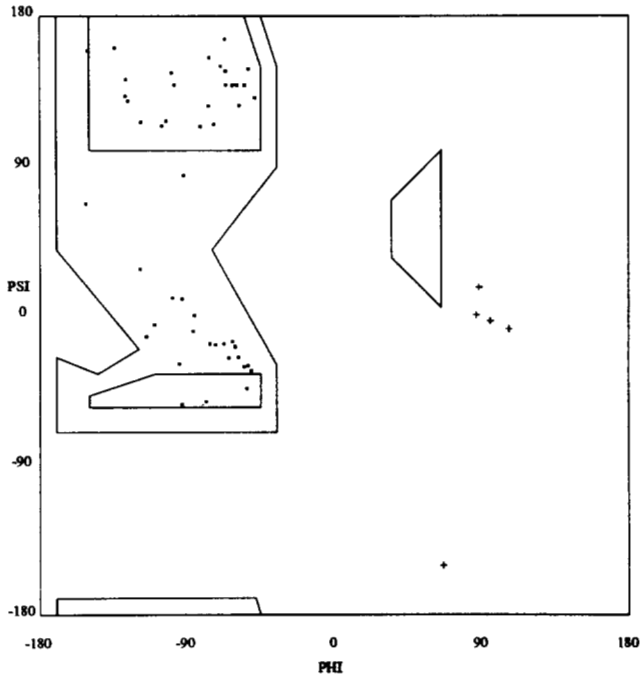

Fig. 5. Ramachandran plot for the oxidized form of RdPf. Glycine residues are indicated by +.

ble 1) with the exception of position 3 (this is equivalent to position 4 in all other rubredoxins due to the lack of an N-terminal methionine residue in RdPf), which is Trp in RdPf and in the rubredoxin from *Clostridium thermosaccharolyticum*, and either Tyr or Phe in all other rubredoxins. The hydrophobic aliphatic side chain at position 32 is either Leu, Ile, or Val in all known rubredoxins.

Numerous turns are present in the RdPf structure. Of those turns stabilized by hydrogen bonds between the CO of residue n and the NH of residue $n + 3$ (Venkatachalam, 1968), the two most prevalent types are the common turn and the glycine turn (Richardson, 1981; Richardson & Richardson, 1989). Overlapping common turns occur between residues 13–17, 18–22, 28–32, and 44–48 (for examples, see Kinemage 4). These successive turns approximate stretches of a 3_{10}-helix and were described by Watenpaugh et al. (1979) as forming helical corners in the RdCp structure. Other turns include residues 24–27 (forming a glycine turn) and 33–36 (forming a common turn). Additionally, residues Asp 13 to Asp 15 form an Asx turn (Richardson, 1981; Rees et al., 1983), which resembles a reverse turn in which an Asp 13 side chain carboxyl oxygen forms a hydrogen bond with the amide nitrogen of Asp 15.

Iron–sulfur environment

The sulfur atoms of the four cysteine residues ligand the iron atom with nearly equal bond lengths (see Table 3), forming an approximately tetrahedral coordination sphere. As noted by Watenpaugh et al. (1979), an approximate twofold axis relates two loops of the polypeptide chain, one consisting of residues 4–11, and the other of residues 37–44 (Fig. 10; Kinemage 2). Furthermore, this approximate twofold axis is reflected in the pattern of the S-Fe-S bond angles (see Table 3). Additionally, the cluster environment includes six N-H···Sγ hydrogen bonds (see Table 2 and Kinemage 1), two to C5Sγ from I7NH and C8NH, two to C38Sγ from I40NH and C41NH, and one each to C8Sγ from Y10NH and to C41Sγ from A43NH. This network of hydrogen bonds also reflects the approximate twofold symmetry about the cluster.

Comparison of oxidized and reduced forms

As noted above, there are few differences between the structures of the oxidized and reduced forms of RdPf (see Kinemage 1), which is reflected in a rms difference in Cα coordinates of 0.27 Å. By minimizing the confor-

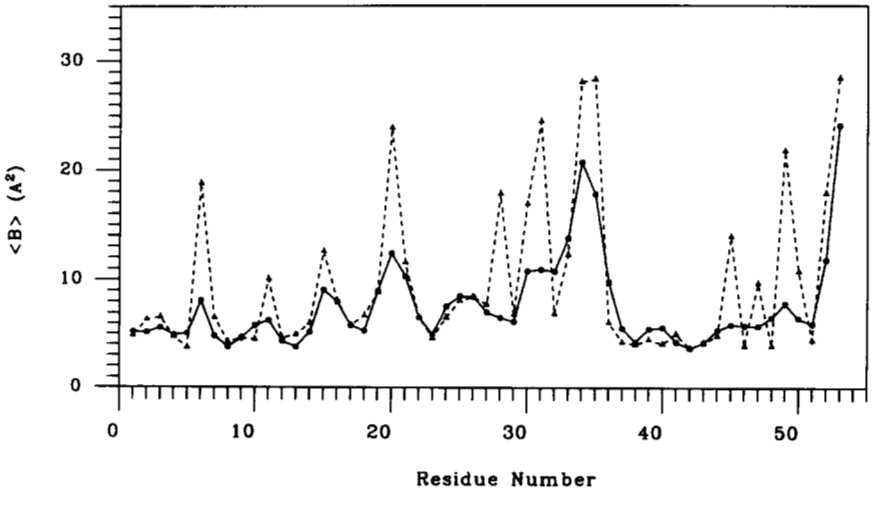

Fig. 6. Average main chain and side chain temperature factors for the reduced form. The main chain is shown by the solid line and the side chain is shown by the dashed line.

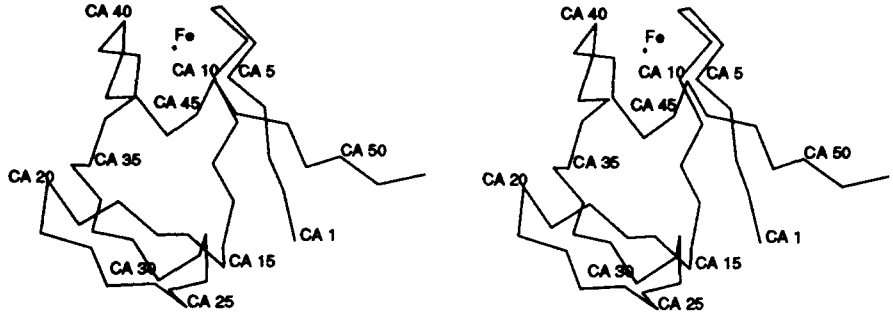

Fig. 7. Cα trace showing the overall folding of RdPf. The iron atom is at the top of the molecule with the sheet to the right. The pendant tail on the right is the C-terminus.

mational changes associated with oxidation/reduction, electron transfer reactions involving rubredoxin should be kinetically facilitated. Reduction of RdPf is accompanied by an increase in the iron–sulfur bond lengths by an average of 0.04 Å (see Table 3). It should be noted that these bond lengths were not restrained during refinement, and although the difference in bond lengths between the reduced and oxidized forms is within the estimated coordinate error, there is a consistent increase for all four of them. There is also a decrease in the average NH···S hydrogen bond distance by 0.09 Å upon reduction (see Table 3). This shortening would help stabilize the negative charge introduced upon reduction and is consistent with an observed shortening of the N···S distances upon reduction of the oxidized form of the high-potential iron protein (Carter et al., 1974). Although of doubtful functional relevance, the quantitatively most significant difference between oxidized and reduced RdPf in the crystals occurs at the C-terminus. The positions of the Cα of Asp 53 differ by 1.38 Å between the two forms with even larger differences observed for the side chain atoms. This residue makes an intermolecular contact with a neighboring molecule. Additionally, there is a hydrogen bond between the amide nitrogen of Glu 52 in the reduced molecule and the carbonyl oxygen of Ile 40 in a neighboring molecule. This lattice contact is near Cys 41, which is an iron-liganding residue. It is possible that reduction of the protein in the crystalline state disturbs this lattice contact, thereby accounting for the extremely fragile nature of the reduced crystal. None of the other intermolecular contacts exhibit a similar displacement.

Comparison to other rubredoxins of known structure

The overall folding, the environment around the iron atom, the hydrophobic core, and the hydrogen bonding network of RdCp, RdDd, RdDv, RdDg, and RdPf are extremely similar. The rms deviation in the Cα atomic positions between RdPf and the other rubredoxins – RdCp, RdDd, RdDv, and RdDg – are 0.47 Å, 0.69 Å, 0.56 Å, and 0.63 Å, respectively. The deviations for the Cαs of the aromatic residues in the conserved hydrophobic core are 0.29 Å, 0.39 Å, 0.33 Å, and 0.27 Å, respectively. Chothia and Lesk (1986) have observed that the coordinate divergence, Δ, between two structures can be estimated from their fractional sequence difference, H, by the relationship:

$$\Delta = 0.40e^{1.87H}, \quad (1)$$

where Δ is measured in Å. The fractional sequence differences (H) between RdPf and RdCp, RdDd, RdDv, and RdDg are 0.42 (22/52), 0.55 (25/45), 0.35 (18/52), and 0.35

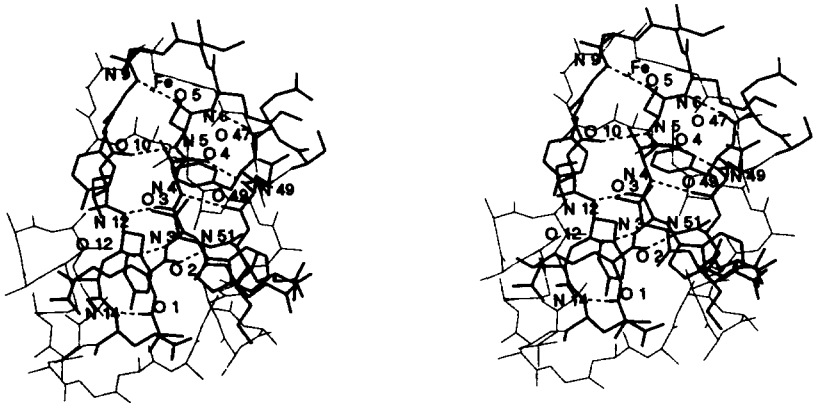

Fig. 8. Stereo view of the hydrogen-bonding network in the β-sheet including the hydrogen bond, O5···N9, that defines a G-1 β-bulge.

Table 2. *Hydrogen bonds observed between protein atoms in Pyrococcus furiosus rubredoxin*

Donor	Acceptor	Oxidized (Å)	Reduced (Å)
	Main chain to main chain		
W3N	Y12O	2.9	2.9
V4N	E49O	2.8	2.8
C5N	Y10O	2.9	2.8
K6N	E47O	2.8	2.8
G9N	C5O	2.9	3.0
Y12N	W3O	2.7	2.8
E14N	A1O	3.0	3.0
A16N	D13O	2.8	2.9
G17N	D13O	3.0	2.9
D18N	I23O	3.0	2.9
N21N	D18O	2.9	2.9
G22N	P19O	3.2	3.0
I23N	D18O	3.0	3.0
G26N	E14O	2.8	2.8
T27N	S24O	3.3	3.3
E31N	K28O	2.9	2.8
L32N	F29O	3.1	3.0
W36N	P33O	2.9	2.9
C38N	A43O	2.9	2.9
G42N	C38O	2.9	2.9
E47N	P44O	3.0	2.9
F48N	K45O	3.0	3.0
E49N	V4O	2.8	2.9
L51N	K2O	2.8	2.8
E52N	K50O	3.1	3.2
	Nitrogen–sulfur		
I7N	C5Sγ	3.52	3.34
C8N	C5Sγ	3.58	3.42
Y10N	C8Sγ	3.47	3.41
I40N	C38Sγ	3.42	3.36
C41N	C38Sγ	3.52	3.46
A43N	C41Sγ	3.49	3.50
	Side chain to main chain		
Y12Oη	T27O	2.6	2.6
D15N	D13Oδ1	2.9	2.9
A1N	E14Oε2	2.9	2.9
F29N	E14Oε1	2.8	2.9
T27Oγ1	S24O	2.8	2.7
E30N	E30Oε2	2.7	2.8
K45Nζ	F29O	3.0	2.8
K45Nζ	L32O	2.8	3.5
	Side chain to side chain		
W3Nε1	E14Oε1	3.4	3.4
K6Nζ	E49Oε2	2.6	4.1
W36Nε1	D18Oδ2	2.9	3.0
N21Nδ2	D18Oδ1	3.0	3.2
S46Oγ	E47Oε2	2.7	2.7

Table 3. *Bond distances and bond angles in the iron–sulfur cluster*

				Oxidized	Reduced
		Bond distances to iron (Å)[a]			
C5Sγ	Fe			2.31	2.34
C8Sγ	Fe			2.25	2.29
C38Sγ	Fe			2.33	2.36
C41Sγ	Fe			2.25	2.29
		Bond angles around Fe (degrees)			
C5Sγ	Fe	C8Sγ		113.4	112.2
C5Sγ	Fe	C38Sγ		112.0	113.8
C5Sγ	Fe	C41Sγ		102.6	104.7
C8Sγ	Fe	C38Sγ		102.2	102.7
C8Sγ	Fe	C41Sγ		115.1	111.4
C38Sγ	Fe	C41Sγ		112.1	112.6
		Torsion angles about SG (degrees)			
Fe	C5Sγ	C5Cβ	C5Cα	169°	179°
Fe	C8Sγ	C8Cβ	C8Cα	90°	87°
Fe	C38Sγ	C38Cβ	C38Cα	169°	176°
Fe	C41Sγ	C41Cβ	C41Cα	88°	87°

[a] The iron–sulfur distance force constant in X-PLOR was set to zero during refinement.

(18/51), respectively, which correspond to calculated Δ values of 0.87 Å, 1.13 Å, 0.76 Å, and 0.77 Å, respectively. Therefore, the observed structural similarities are consistent with the general degree of sequence conservation observed in the rubredoxin family.

Despite the overall similarities, there are differences between the rubredoxin structures that may contribute to the thermostability of RdPf. For the purposes of comparing the RdPf structure to other rubredoxins, it is convenient to focus on three features: main chain to main chain hydrogen bonds, buried surface area, and amino acid residues unique to RdPf. In this discussion, the assumption is made that RdPf is more stable than the other rubredoxins of known structure. As mentioned in the introduction, it appears that RdPf is more stable than RdCp (Lovenberg & Sobel, 1965) and RdDg (Papavassilou & Hatchikian, 1985). No studies of the stabilities of either RdDd and RdDv have apparently been reported. Consequently, although it is reasonable to assume that RdPf is more stable than the rubredoxins from mesophilic organisms, this has not been rigorously established.

Main chain to main chain hydrogen bonds

Relative to other rubredoxins, RdPf has a more extensive network of main chain to main chain hydrogen bonds. In RdPf, the β-sheet hydrogen-bonding network extends up to residue 1 (Kinemage 4), whereas in RdCp, RdDd, RdDv, and RdDg, the hydrogen-bonding network stops at residue 3. Extension of the hydrogen-bonding network to the amino-terminus permits formation of two additional β-sheet hydrogen bonds: one between the carbonyl oxygen of Ala 1 and the amide nitrogen of Glu 14, and the second between the carbonyl oxygen of Lys 2 and the amide nitrogen of Leu 51. Relative to mesophilic rubredoxins, the more extensively hydrogen-bonded β-sheet in RdPf could enhance the stability of this structure against thermal disruption.

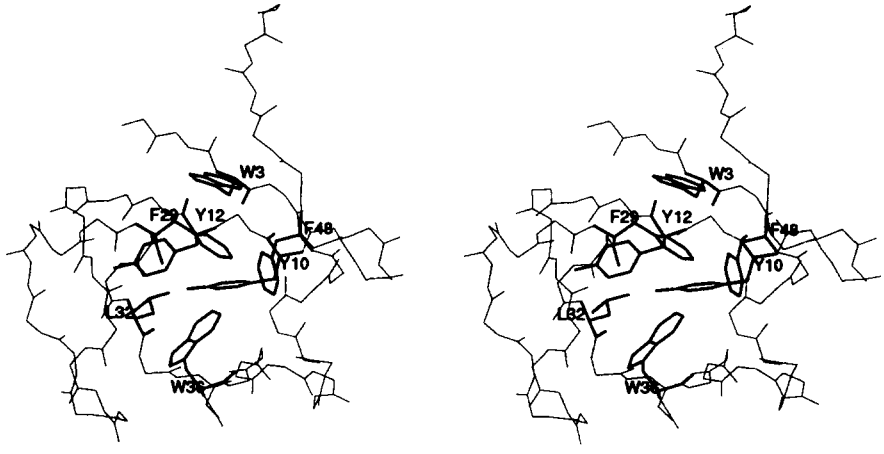

Fig. 9. Stereo view of the aromatic residues and Leu 32 that form the hydrophobic core of RdPf.

Buried surface area

The contribution of hydrophobic interactions, ΔG_H, to protein stability has been characterized by analysis of the amount and type of protein surface area that becomes buried during protein folding (Chothia, 1974). In general, ΔG_H is expressed as the product of two terms: (1) the surface area of the region buried from exposure to water during folding and (2) a surface free energy term. In a method developed by Eisenberg and McLachlan (1986), ΔG_H may be expressed as a sum involving the difference in solvent-accessible surface area (Richards, 1977) of the ith atom, A_i, between the folded and unfolded states, and the surface free energy, $\Delta\sigma_i$, for each atom type:

$$\Delta G_H = \sum_i \Delta\sigma_i [A_i(\text{folded}) - A_i(\text{unfolded})], \qquad (2)$$

where the sum is over all atoms i. The surface free energies of transfer between the protein interior and the aqueous phase for different atom types are (in cal $Å^{-2}$) $\Delta\sigma(C) = 18$, $\Delta\sigma(N/O) = -9$, $\Delta\sigma(O^-) = -37$, $\Delta\sigma(N^+) = -38$, $\Delta\sigma(S) = -5$ (Eisenberg et al., 1989). Accessible surface areas were calculated from rubredoxin coordinates with the program ACCESS (Lee & Richards, 1971), using van der Waals radii for various atom types taken from Chothia (1976). The accessible surface areas of atoms in a hypothetical unfolded state are taken from Eisenberg et al. (1989). The results of these calculations for the five different rubredoxin structures are presented in Table 4. RdPf exhibits the greatest calculated contribution to protein stability from these hydrophobic interactions, as a consequence of burying the greatest amount of nonpolar (carbon) surface area. The difference between ΔG_H for RdPf and some of the other rubredoxin structures, most noticeably RdCp, is not large, however, suggesting that other factors must also contribute to the thermostability of RdPf. There does not appear to be anything unusual about the surface areas exposed to water in the folded rubredoxin structures, as the total areas are close to those anticipated for water-soluble globular proteins of comparable molecular weight, and the fraction of the exposed surface contributed by carbon atoms is also typical for water-soluble globular proteins (Miller et al., 1987). The fraction of the buried surface area that is nonpolar in RdPf (~70%) is greater than that generally observed for water-soluble globular proteins (~58%) (Miller et al., 1987), but this fraction does not vary significantly between the different rubredoxin structures.

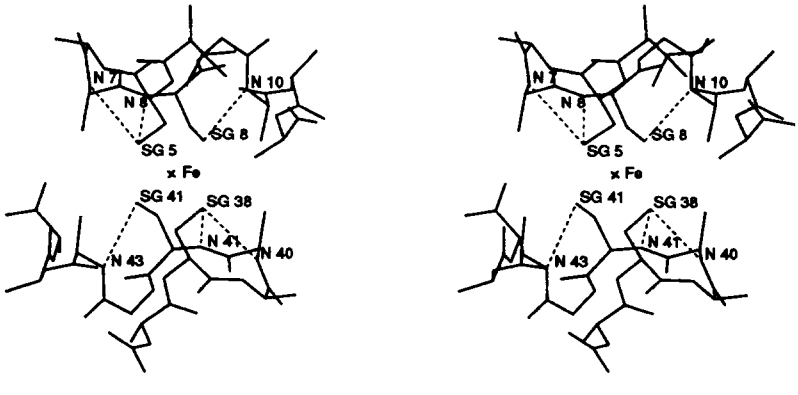

Fig. 10. Stereo view of the pseudo-twofold axis around the iron-sulfur cluster.

Table 4. *Buried and exposed accessible surface areas for rubredoxins*[a]

	A_{total} (Å^2)[b]	A_{NP} (Å^2)[c]	A_{buried} (Å^2)[d]				ΔG_H[e] (kcal/mol)
			C	N/O	O^-/N^+	S	
RdPf	3,398	1,884	3,637	1,223	197	106	−46.5
RdCp	3,572	1,917	3,580	1,178	195	129	−45.9
RdDg	3,325	1,809	3,438	1,186	175	126	−44.0
RdDv	2,887	1,902	3,335	1,167	206	141	−41.0
RdDd	3,029	1,520	2,997	1,042	71	125	−41.2

[a] For key to abbreviations of rubredoxins, see Figure 1.
[b] Total exposed surface area.
[c] Nonpolar (carbon) exposed surface area.
[d] Buried surface area for carbon atom (C), uncharged nitrogen/oxygen atoms (N/O), charged oxygen/nitrogen atoms (O^-/N^+), and sulfur atoms (S).
[e] Calculated contribution of hydrophobic energies to free energy of folding (Equation 2).

Amino acid residues unique to RdPf

The interactions of the Glu 14 side chain with groups on three other residues: the amino terminal nitrogen of Ala 1, the indole nitrogen of Trp 3, and the NH group of Phe 29 are shown in Figure 11 (Kinemage 5; the residue numbering scheme is based on the RdPf sequence [Fig. 1]). This could only occur in RdPf, as this is the only rubredoxin of known sequence that simultaneously contains Ala 1, Trp 3, and Glu 14. Although the Glu 14 Oε1 to Trp 3 Nε1 distance (3.45 Å) is long for a hydrogen bond, the relative orientations of these two groups indicate that a favorable electrostatic interaction does occur. Interestingly, the only other rubredoxin known to contain a tryptophan residue at position 3 has been isolated from the thermophilic eubacterium *C. thermosaccharolyticum* (Devanathan et al., 1969; Tanaka et al., 1971; Fig. 1). This rubredoxin does not contain Glu 14, however. The only other rubredoxin to contain a glutamate at position 14 (isolated from *Megasphaera elsdenii* [Fig. 1]) contains neither Ala 1 nor Trp 3. The presence of this residue in RdPf that interconnects Ala 1, Trp 3, Glu 14, and Phe 29 is consistent with the idea that an increased number of salt bridges and other electrostatic interactions can enhance thermostability (Perutz, 1978). The presence of another residue uniquely found in RdPf (Lys 6) is also consistent with this idea, as this side chain is observed to form a salt bridge with the Glu 49 side chain.

Thermodynamic origins of hyperthermostability

A central issue in the analysis of hyperthermostable proteins concerns the thermodynamic details of protein stability. A fundamental, yet presently unanswered, question is the degree to which the stabilities of hyperthermostable proteins are enhanced relative to mesophilic proteins. Calorimetric techniques are the method of choice for addressing questions of protein stability. Although detailed calorimetric studies of the stability of hyperthermophilic proteins have not been described, some general considerations may be derived from the behavior of small, water-soluble, mesophilic proteins (Privalov, 1979, 1989; Privalov & Gill, 1988). Thermodynamically, the unfolding of these proteins can often be characterized in terms of a transition between two states, the native (N) and an unfolded, denatured form (D). The free energy of unfolding from the N to D states, ΔG_{ND}, is often observed to be about 10–15 kcal/mol under conditions of maximal stability.

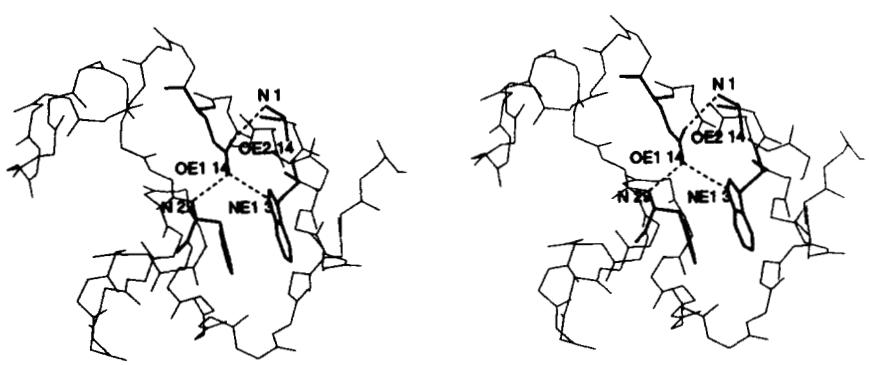

Fig. 11. Stereo view of the hydrogen bonds and salt bridge formed by Glu 14.

The unfolding transition is associated with a large, positive change in the heat capacity, ΔC_p, which reflects exposure of apolar groups to water during unfolding. To a first approximation, ΔC_p is temperature independent, although this assumption becomes less valid at higher temperatures where ΔC_p decreases.

For a two-state process with constant ΔC_p, ΔG_{ND} may be expressed as:

$$\Delta G_{ND} = \Delta H_m\left[\frac{T_m - T}{T_m}\right] - \Delta C_p\left[T_m - T\left(1 - \ln\left(\frac{T}{T_m}\right)\right)\right], \quad (3)$$

where T_m is the transition temperature for unfolding during heat denaturation (the temperature at which $\Delta G_{ND} = 0$); and ΔH_m is the enthalpy change at T_m. The entropy change at T_m is given by $\Delta S_m = \Delta H_m/T_m$. Assuming ΔC_p is temperature independent, ΔG_{ND} is completely specified by the three parameters, T_m, ΔH_m, and ΔC_p, or equivalently, ΔH_m, ΔS_m, and ΔC_p. The dependence of ΔG_{ND} on T for a given set of solution conditions (pH, ionic strength, etc.) defines the stability curve for a protein (Becktel & Schellman, 1987).

The dependence of ΔG_{ND} on ΔH_m, T_m, and ΔC_p can be more easily appreciated from an approximate expression derived by expanding Equation 3 to second order in $(T_m - T)$:

$$\Delta G_{ND} \cong \left[\Delta H_m - \frac{(\Delta C_p)T_m}{2}\right] + T\left[\Delta C_p - \frac{\Delta H_m}{T_m}\right] - T^2\left[\frac{\Delta C_p}{2T_m}\right]. \quad (4)$$

This quadratic form implies that there are, in general, two temperatures for which $\Delta G_{ND} = 0$: one at $T = T_m$ (heat denaturation), characterized by ΔH_m, $\Delta S_m > 0$, and a lower temperature $T = T_m - 2[\Delta H_m/\Delta C_p]$ (cold denaturation), characterized by ΔH_m, $\Delta S_m < 0$. The process of cold denaturation has been experimentally observed (Privalov, 1990). Consequently, within the framework of this approximate treatment, the native form of a protein is thermodynamically stable over a temperature range $\Delta T \sim 2[\Delta H_m/\Delta C_p]$.

From Equation 4, the temperature of greatest protein stability, T^*, for $\Delta C_p > 0$, occurs when

$$T^* \cong T_m - \left[\frac{\Delta H_m}{\Delta C_p}\right], \quad (5)$$

with the free energy of maximal stability given by:

$$\Delta G_{ND}(T^*) \cong \left[\frac{\Delta H_m^2}{2T_m\Delta C_p}\right] = \left[\frac{\Delta H_m \Delta S_m}{2\Delta C_p}\right]. \quad (6)$$

For the hypothetical "typical" water-soluble protein, $\Delta H_m = 100$ kcal/mol, $T_m = 340$ K, and $\Delta C_p = 2$ kcal/mol/K, giving $T^* = 290$ K and $\Delta G_{ND}(T^*) = 7.4$ kcal/mol. The corresponding quantities for hyperthermostable proteins are unknown, except that $T_m > 370$ K.

Based on these considerations, hyperthermostability can in principle be achieved by some combination of increasing ΔH_m and/or decreasing ΔS_m and/or ΔC_p. There are few a priori restrictions on how these changes are accomplished, provided that $\Delta H_m/\Delta S_m = T_m > \sim 370$ K. Possible mechanisms for enhancing the thermostability of proteins by alterations in ΔH_m, ΔS_m, and ΔC_p will be briefly discussed. The emphasis in this discussion is on interactions that stabilize the native state, since these can in principle be characterized from the native structure. It is also possible, however, that protein stability reflects contributions from unfolded forms (Dill & Shortle, 1991) that cannot be addressed in this study.

ΔH_m

The temperature dependence of the specific enthalpy of unfolding (enthalpy per gram) of several small, globular proteins intersect at a common value of about 13 cal/g at a temperature $T \sim 110$ °C. Privalov (1979) has suggested that this intercept represents the contribution to protein stabilization from nonhydrophobic sources, such as hydrogen bonding, and that the value of 13 cal/g is characteristic of compact, globular proteins. The iron ligation presumably provides a strong, stabilizing interaction for the native state, although given the similarity in metal sites between different rubredoxins, this would not be expected to provide the dominant mechanism of thermostability in RdPf relative to other rubredoxins. The observation that the RdPf has a more extensive hydrogen-bonding network within the protein than other rubredoxins of known structure suggests that this may contribute to the stability by increasing the enthalpy of unfolding.

ΔS_m

Under conditions where ΔG_{ND} is pH independent, the entropy of unfolding will consist of contributions from two sources (Privalov, 1979): (1) the change in the number of conformational degrees of freedom upon unfolding, and (2) hydration effects arising from exposure of buried groups to water. Substitutions for glycines and prolines within a sequence have been proposed as a mechanism to alter protein stability by manipulating the entropy of the unfolded state (Nemethy et al., 1966; Hecht et al., 1986; Matthews et al., 1987). Two such changes occur within the rubredoxin family that may be relevant to the stability of RdPf: residue 14, which is Glu in RdPf, but Pro in nearly every other rubredoxin; and residue 44, which is Pro in both RdPf and RdDv, but Gly in RdCp and Ser in RdDg and RdDd. The first change, substitution of Glu 14 for Pro in RdPf, would be expected to decrease thermostability by increasing ΔS_m by up to 2.4

cal/mol/K (equivalent to decreasing $-T_m\Delta S_m$ by almost 1 kcal/mol), but this could be offset by favorable energetic interactions between Glu 14 and three other residues. Incorporation of Pro 44 into RdPf could stabilize the protein by decreasing ΔS_m up to 4 cal/mol/K (corresponding to increasing $-T_m\Delta S_m$ by about 2.4 kcal/mol). Hence, this latter substitution might reasonably contribute to the stability of RdPf. Contributions to unfolding entropy from hydration effects are discussed in the next section.

ΔC_p

The large ΔC_p associated with the unfolding of small, globular, mesophilic proteins is believed to reflect the involvement of hydrophobic interactions in protein stability. For example, the magnitude of ΔC_p has been shown to be proportional to the number of nonpolar contacts within a protein (Privalov, 1979) or equivalently, to the amount of nonpolar surface area buried within a protein (Livingston et al., 1991). As noted by Privalov and Gill (1988), however, the phenomenon of cold denaturation reflects the decreased stability of a protein as ΔC_p increases. For example, a protein for which $\Delta C_p \leq 0$ would not undergo cold denaturation. Consequently, a decrease in ΔC_p for protein unfolding will contribute to an increase in protein stability (Equation 6). In principle, a decrease in ΔC_p could be accomplished by either minimizing the exposure of apolar groups to water during unfolding (which is associated with a positive ΔC_p), or by increasing the contribution of unfolding processes that are associated with negative ΔC_p (such as the exposure of charged groups during unfolding [Sturtevant, 1977]). There is no compelling evidence for the contribution of either mechanism to the stability of RdPf. Because the amount of nonpolar surface area calculated in RdPf to be buried upon folding is similar to other proteins of comparable size, ΔC_p associated with hydrophobic effects should also be similar (Livingston et al., 1991). Furthermore, the observation that only approximately two intramolecular salt bridges are present in the different rubredoxins (about that expected for a typical protein the size of rubredoxin) (Barlow & Thornton, 1983) indicates that exposure of charged groups during unfolding will not make a significant contribution to ΔC_p.

Although there are a few more hydrogen bonds and somewhat more nonpolar surface area estimated to be buried upon folding in RdPf than other rubredoxins, there is no evidence for large differences in the number of stabilizing interactions, or for new types of interactions that are responsible for RdPf stability. This suggests that it is unlikely that there are enormous differences in stabilization energies for RdPf relative to mesophilic rubredoxins. Although these considerations are qualitative, it would seem that ΔH_m, ΔS_m, and ΔC_p for RdPf are more likely to be within a factor of 2 of the values for mesophilic rubredoxins, than to differ by more than a factor of 10. From Equation 6, this implies that the maximum stability of RdPf relative to mesophilic rubredoxins is also more likely to be within a factor of 2 than to be greater than a factor of 10. It is, of course, imperative that these qualitative speculations be replaced with actual experimental values for rubredoxin stabilities.

Conclusions

Hyperthermostability in RdPf is achieved with minimal alterations to the basic rubredoxin fold. Strikingly, the hydrophobic core of RdPf exhibits significant sequence conservation and structural similarity with the rubredoxins from mesophilic organisms. Most of the unique interactions that occur in RdPf, and which presumably contribute to the stability of this protein, involve electrostatic interactions between groups near the protein surface. This suggests that protein thermostability can be accomplished by appropriate modification of surface residues. From a practical standpoint, this should be more easily accomplished than alterations to the protein interior. Of critical need in the analysis of protein thermostability are quantitative experimental studies using homologous mesophilic and hyperthermophilic proteins, that address such basic questions as "How stable are (hyper)thermostable proteins and why?" A combination of calorimetric, structural and molecular biological studies of hyperthermostable proteins holds great promise for both defining the structural origins of protein stability and permitting its rational modification.

Acknowledgments

We thank A.J. Chirino for his advice and assistance throughout the course of this research. This work was supported by grants from the National Science Foundation DMB-9118689 (D.C.R), and BCS-9011583 (M.W.W.A.), the Office of Naval Research N00014-90-J-1894 (M.W.W.A.), and by a National Science Foundation Training Group Award to the Center for Metalloenzyme Studies of the University of Georgia DIR-9014281. We also acknowledge the Department of Education (M.W.D.) and a Weizmann postdoctoral fellowship (L.J.) for support.

References

Abola, E.E., Bernstein, F.C., Bryant, S.H., Koetzle, T.F., & Weng, J. (1987). Protein Data Bank. In *Crystallographic Databases—Information Content, Software Systems, Scientific Applications* (Allen, F.H., Bergerhoff, G., & Sievers, R., Eds.), pp. 107–132. International Union of Crystallography, Bonn/Cambridge/Chester.

Adman, E.T. (1990). A tale of four iron–sulfur proteins: Sequence errors and other matters. In *Accuracy and Reliability of Macromolecular Crystal Structures* (Henrick, K., Moss, D.S., & Tickle, I.J., Eds.), pp. 97–101. Science & Engineering Research Council, Daresbury Laboratory, Warrington.

Adman, E.T., Sieker, L.C., & Jensen, L.H. (1991). Structure of rubredoxin from *Desulfovibrio vulgaris* at 1.5 Å resolution. *J. Mol. Biol. 217*, 337–352.

Bachmeyer, H., Benson, A.M., Yasunobo, K.T., Garrad, W.T., & Whitely, H.R. (1968a). Non-heme iron proteins. IV. Structural studies of *Micrococcus aerogenes* rubredoxin. *Biochemistry 7*, 986–996.

Bachmeyer, H., Yasunobo, K.T., Peel, J.L., & Mayhew, S. (1968b). Nonheme iron proteins *J. Biol. Chem. 243*, 1022–1030.

Barlow, D.J. & Thornton, J.M. (1983). Ion-pairs in proteins. *J. Mol. Biol. 168*, 867-885.
Becktel, W.J. & Schellman, J.A. (1987). Protein stability curves. *Biopolymers 26*, 1859-1877.
Bernstein, F.C., Koetzle, T.F., Williams, G.J.B., Meyer, E.F., Jr., Brice, M.D., Rodgers, J.R., Kennard, O., Shimanouchi, T., & Tasumi, M. (1977) The Protein Data Bank: A computer-based archival file for macromolecular structures. *J. Mol. Biol. 112*, 535-542.
Bethge, P. (1984). VAX adaptation of the ROCKS crystallographic program system. *J. Appl. Crystallogr. 17*, 215.
Blake, P.R., Park, J.-B., Bryant, F.O., Aono, S., Magnuson, J.K., Eccleston, E., Howard, J.B., Summers, M.F., & Adams, M.W.W. (1991). Determinants of protein hyperthermostability: Purification and amino acid sequence of rubredoxin from the hyperthermophilic archaebacterium *Pyrococcus furiosus* and secondary structure of the zinc adduct by NMR. *Biochemistry 30*, 10885-10895.
Brünger, A.T., Krukowski, A., & Erickson, J.W. (1990). Slow-cooling protocols for crystallographic refinement by simulated annealing. *Acta Crystallogr. 46*, 585-593.
Brünger, A.T., Kuriyan, J., & Karplus, M. (1987). Crystallographic R factor refinement by molecular dynamics. *Science 235*, 458-460.
Bruschi, M. (1976a). The amino acid sequence of rubredoxin from the sulfate reducing bacterium, *Desulfovibrio gigas*. *Biochem. Biophys. Res. Commun. 70*, 615-621.
Bruschi, M. (1976b). Non-heme iron proteins. The amino acid sequence of rubredoxin from *Desulfovibrio vulgaris*. *Biochim. Biophys. Acta 434*, 4-17.
Bryant, F.O. & Adams, M.W.W. (1989). Characterization of hydrogenase from the hyperthermophilic archaebacterium, *Pyrococcus furiosus*. *J. Biol. Chem. 264*, 5070-5079.
Carter, C.W., Kraut, J., Jr., Freer, S.T., & Alden, R.A. (1974). Comparison of oxidation-reduction site geometries in oxidized and reduced *Chromatium* high potential iron protein and oxidized *Peptococcus aerogenes* ferredoxin. *J. Biol. Chem. 249*, 6339-6346.
Chothia, C. (1974). Hydrophobic bonding and accessible surface area in proteins. *Nature 248*, 338-339.
Chothia, C. (1976). The nature of the accessible and buried surfaces in proteins. *J. Mol. Biol. 105*, 1-14.
Chothia, C. & Lesk, A.M. (1986). The relation between the divergence of sequence and structure in proteins. *EMBO 5*, 823-826.
Crowther, R.A. (1972). A method of positioning a known molecule in an unknown crystal structure. In *The Molecular Replacement Method* (Rossman, M.G., Ed.), pp. 173-178. Gordon and Breach, New York.
Devanathan, T., Akagi, J.M., Hersh, R.T., & Himes, R.H. (1969). Ferredoxin from two thermophilic clostridia. *J. Biol. Chem. 244*, 2846-2853.
Dill, K. & Shortle, D. (1971). Denatured states of proteins. *Annu. Rev. Biochem. 60*, 795-825.
Eisenberg, D. & McLachlan, A.D. (1986). Solvation energy in protein folding and binding. *Nature 319*, 199-203.
Eisenberg, D., Wesson, M., & Yamashita, M. (1989). Interpretation of protein folding and binding with atomic solvation parameters. *Chem. Scrip. 29A*, 217-221.
Fiala, G. & Stetter, K.O. (1986). *Pyrococcus furiosus* represents a novel genus of heterotropic archaebacteria growing optimally at 100 °C. *Arch. Microbiol. 145*, 56-61.
Frey, M., Sieker, L., Payan, F., Haser, R., Bruschi, M., Pepe, G., & LeGall, J. (1987). Rubredoxin from *Desulfovibrio gigas*. A molecular model of the oxidized form at 1.4 Å resolution. *J. Mol. Biol. 197*, 525-541.
Hecht, M.H., Sturtevant, J.M., & Sauer, R.T. (1986). Stabilization of λ repressor against thermal denaturation by site-directed Gly → Ala changes in α-helix 3. *Proteins 1*, 43-46.
Hope, H. (1988). Cryocrystallography of biological macromolecules: a generally applicable method. *Acta Crystallogr. B44*, 22-26.
Hope, H. (1990). Crystallography of biological macromolecules at ultra-low temperature. *Annu. Rev. Biophys. Biophys. Chem. 19*, 107-126.
Hormel, S., Walsh, K.A., Prickril, B.C., Titani, K., & LeGall, J. (1986). Amino-acid sequence of rubredoxin from *Desulfovibrio desulfuricans* strain 27774. *FEBS Lett. 201*, 147-150.
Howard, A.J., Gilliland, G.L., Finzel, B.C., Poulos, T.L., Ohlendorf, D.H., & Salemme, F.R. (1987). The use of an imaging proportional counter in macromolecular crystallography. *J. Appl. Crystallogr. 20*, 383-387.
Jones, A.T. (1978). A graphics model building and refinement system for macromolecules. *J. Appl. Crystallogr. 11*, 268-272.
Lee, B. & Richards, F.M. (1971). The interpretation of protein structures: Estimation of static accessibility. *J. Mol. Biol. 55*, 379-400.
Livingston, J.R., Spolar, R.S., & Record, M.T. (1991). Contributions to the thermodynamics of protein folding from the reduction in water-accessible nonpolar surface area. *Biochemistry 30*, 4237-4244.
Lovenberg, W. & Sobel, B.E. (1965). Rubredoxin: A new electron transfer protein from *Clostridium pasteurianum*. *Proc. Natl. Acad. Sci. USA 54*, 193-199.
Luzzati, V. (1952). Traitement statistique des erreurs dans la determination des structures cristallines. *Acta Crystallogr. 5*, 802-810.
Matthews, B.W. (1968). Solvent content of protein crystals. *J. Mol. Biol. 33*, 491-497.
Matthews, B.W., Nicholson, H., & Becktel, W.J. (1987). Enhanced protein thermostability from site-directed mutations that decrease the entropy of unfolding. *Proc. Natl. Acad. Sci. USA 84*, 6663-6667.
Meyer, J., Gagnon, J., Sieker, L.C., van Dorsselaer, A., & Moulis, J.-M. (1990). Rubredoxin from *Clostridium thermosaccharolyticum*: Amino acid sequence, mass-spectrometric and preliminary crystallographic data. *Biochem. J. 271*, 839-841.
Miller, S., Janin, J., Lesk, A.M., & Chothia, C. (1987). Interior and surface of monomeric proteins. *J. Mol. Biol. 196*, 641-656.
Nemethy, G., Leach, S.J., & Scheraga, H.A. (1966). The influence of amino acid side chains on the free energy of helix-coil transitions. *J. Phys. Chem. 70*, 998-1004.
Papavassilou, P. & Hatchikian, E.C. (1985). Isolation and characterization of a rubredoxin and a two-[4Fe-4S] ferredoxin *Thermodesulfobacterium commune*. *Biochim. Biophys. Acta 810*, 1-11.
Perutz, M.F. (1978). Electrostatic effects in proteins. *Science 201*, 1187-1191.
Privalov, P.L. (1979). Stability of proteins: Small globular proteins. *Adv. Protein Chem. 33*, 167-241.
Privalov, P.L. (1989). Thermodynamic problems of protein structure. *Annu. Rev. Biophys. Chem. 18*, 47-69.
Privalov, P.L. (1990). Cold denaturation of proteins. *Crit. Rev. Biochem. Mol. Biol. 25*, 281-305.
Privalov, P.L. & Gill, S.J. (1988). Stability of protein structure and hydrophobic interaction. *Adv. Protein Chem. 39*, 191-234.
Reeke, G.N., Jr. (1984). The ROCKS system of computer programs for macromolecular crystallography. *J. Appl. Crystallogr. 17*, 125-130.
Rees, D.C., Lewis, M., & Lipscomb, W.N. (1983). Refined crystal structure of carboxypeptidase A at 1.5 Å resolution. *J. Mol. Biol. 168*, 367-387.
Richards, F.M. (1977). Areas, volumes, packing and protein structure. *Annu. Rev. Biophys. Bioeng. 6*, 151-276.
Richardson, J.S. (1981). The anatomy and taxonomy of protein structure. *Adv. Protein Chem. 34*, 167-339. Academic Press, New York.
Richardson, J.S., Getzoff, E.D., & Richardson, D.C. (1978). The β-bulge: A common small unit of nonrepetitive protein structure. *Proc. Natl. Acad. Sci. USA 75*, 2574-2578.
Richardson, J.S. & Richardson, D.C. (1989). Principles and patterns of protein conformation. In *Prediction of Protein Structure and the Principles of Protein Conformation* (Fasman, E.D., Ed.), pp. 1-98. Plenum, New York
Saeki, K., Yao, Y., Wakabayashi, S., Shen, G.J., Zeikus, J.G., & Matsubara, H. (1989). Ferredoxin and rubredoxin from *Butyribacterium methylotrophicum*: Complete primary structures and construction of phylogenetic trees. *J. Biochem. 106*, 656-662.
Seki, Y., Seki, S., Satoh, M., Ikeda, A., & Ishimoto, M. (1989). Rubredoxin from *Clostridium perfringens*—Complete amino-acid sequence and participation in nitrate reduction. *J. Biochem. 106*, 336-341.
Shimizu, F., Ogata, M., Yagi, T., Wakabayashi, S., & Matsubara, H. (1989). Amino-acid sequence and function of rubredoxin from *Desulfovibrio vulgaris* Miyazaki. *Biochemie 71*, 1171-1177.
Sieker, L.C., Stenkamp, R.E., Jensen, L.H., Prickril, B., & LeGall, J. (1986). Structure of rubredoxin from the bacterium *Desulfovibrio desulfuricans*. *FEBS 208*, 73-76.
Srinivasan, R. & Parthasarathy, S. (1976). *Some Statistical Applications in X-ray Crystallography*. Pergamon Press, Oxford.
Sturtevant, J.M. (1977). Heat capacity and entropy changes in processes involving proteins. *Proc. Natl. Acad. Aci. USA 74*, 2236-2240.
Tanaka, M., Haniu, M., Matsueda, G., Yasunobo, K.T., Himes, R.H., Akagi, J.M., Barnes, E.M., & Devanathan, T. (1971). The primary

structure of the *Clostridium tartarivorum* ferredoxin, a heat-stable ferredoxin. *J. Biol. Chem. 246*, 3953–3960.

Tronrud, D.E., Ten Eyck, L.F., & Matthews, B.W. (1987). An efficient general-purpose least-squares refinement program for macromolecular structures. *Acta Crystallogr. A23*, 489–501.

Venkatachalam, C.M. (1968). Stereochemical criteria for polypeptides and proteins. V. Conformation of a system of three linked peptide units. *Biopolymers 6*, 1425–1436.

Voordouw, G. (1988). Cloning of genes encoding redox proteins of known amino acid sequence from a library of the *Desulfovibrio vulgaris* (Hildenborough) genome. *Gene 67*, 75–83.

Watenpaugh, K.D., Sieker, L.C., Herriot, J.R., & Jensen, L.H. (1973). Refinement of the model of a protein: Rubredoxin at 1.5 Å resolution. *Acta Crystallogr. B29*, 943.

Watenpaugh, K.D., Sieker, L.C., & Jensen, L.H. (1979). The structure of rubredoxin at 1.2 Å resolution. *J. Mol. Biol. 131*, 509–522.

Woolley, K.J. & Meyer, T.E. (1987). The complete amino-acid sequence of rubredoxin from the green phototrophic bacterium *Chlorobium thiosulfatophilum* strain PM. *Eur. J. Biochem. 163*(1), 161–166.

Yasunobo, K.T. & Tanaka, M. (1983). The types, distribution in nature, structure–function, and evolutionary data of the iron–sulfur proteins. In *Iron–Sulfur Proteins* (Lovenberg, W., Ed.), pp. 27–130. Academic Press, New York.